

Hanging nodes in the Context of Algebraic Stabilizations for Convection-Diffusion Equations

Abhinav Jha *

Abstract

In this work, we propose an investigation of hanging nodes in the context of a posteriori error estimator for algebraic flux-corrected (AFC) schemes for stationary convection-diffusion equations. Results have also been presented for the handling of grids with hanging nodes for higher-order Lagrange elements. Numerical simulation illustrating the satisfaction and the violation of discrete maximum principle (DMP) for the BJK limiter and the Kuzmin limiter, respectively have been presented in two dimensions.

Keywords: hanging nodes, steady-state convection-diffusion equations, a posteriori error estimator, algebraic flux correction (AFC) schemes

1 Introduction

If adaptively refined grids based on a posteriori error estimators should be used, then one has to define the actual grid refinement. One would prefer the subsequent grids to hold the same geometrical properties as that of the initial grid, e.g., preservation of angles. Some of the common strategies to refine a grid can be found in [Riv84, BSW83, KR89]. The first step of the refinement of a grid, i.e., the refinement of the marked cells leads to the formation of hanging vertices which can be described as the non-trivial linear combination of the endpoints of the edge to which it belongs. In the framework of discontinuous finite elements, the handling of grids with a hanging vertex is rather easy to understand (see [AR10]). We would like to explicitly point that in existing literature, what we have mentioned as the hanging vertex is referred to as a hanging node (see [CH09]). The distinction between the two would be made clear in the subsequent section. For continuous finite elements, the framework becomes a little involved. One easy way around this is to use conforming closure or red-green refinements (see [BSW83]) but this leads to the deterioration of angles. Also, while using

*Freie Universität Berlin, Department of Mathematics and Computer Science, Arnimallee 6, 14195 Berlin, Germany, jha@wias-berlin.de

hexahedral mesh cells in 3d, the green completion leads to formation of pyramids or prisms, which are not easy to handle by the finite element code and hence one would like to work with hanging vertices.

Certain finite element discretizations rely on the geometrical properties of the grid (see [XZ99, BJK16]) such as angle preservation. Hence, one would like to study a continuous finite element in the framework of grids with hanging nodes. Angle preservation is also an important property for a certain class of stabilization methods for *convection-diffusion-reaction* equations as they provide a sufficient condition for the satisfaction of discrete maximum principle (DMP) (see [BJK16]). To the best of our knowledge, no work has been done in the context of hanging nodes and nonlinear stabilization such as algebraic flux correction schemes (AFC). Some work in the area of hanging nodes can be found in [Grä11] where results have been provided for the lowest order Lagrange elements in the framework of multigrid methods and [CH09] where a unified error analysis for a posteriori error estimation has been provided.

In this work we present the first work regarding the interplay of AFC schemes and grids with hanging nodes. The paper is divided as follows: In Sec. 2 certain definitions and notations would be discussed. In Sec. 3 we extend the results from [Grä11] to higher-order Lagrange elements. Next, in Sec. 4 we present results concerning the behavior of AFC schemes concerning grids with hanging nodes. Finally, numerical simulations illustrating the results provided in the previous section will be presented in Sec. 5.

2 Preliminaries

For $d > 1$, the domain $\Omega \subset \mathbb{R}^d$ is decomposed into (simple) subdomains for which local polynomials are defined. These decompositions are referred as *grids* or *meshes*. A simplicial decomposition, i.e., a decomposition consisting only of triangles or tetrahedra is called a triangulation.

Definition 1. (Grid or Mesh) Let $\Omega \subset \mathbb{R}^d$, $d \in \{2, 3\}$, denote a domain and \mathbb{S} be a finite system of closed connected sets of subdomains of $\overline{\Omega}$. A subset $\mathcal{T} \subset \mathbb{S}$ is called *conformal* if for all $K_1, K_2 \in \mathcal{T}$ with $K_1 \cap K_2 \in \mathcal{T}$ also $K_1 = K_2$ holds. Let $\mathcal{T} = \{K \in \mathbb{S} : \text{int}(K) \neq \emptyset\}$ denote the set of all mesh cells. \mathbb{S} is called a grid or mesh whenever the following property holds:

1. \mathcal{T} covers Ω , i.e., $\overline{\Omega} = \bigcup_{K \in \mathcal{T}} K$,
2. \mathcal{T} is conformal,
3. $\mathbb{S} \cup \partial\Omega$ is closed under intersection of sets, i.e., $K_1, K_2 \in \mathbb{S} \cup \partial\Omega \Rightarrow K_1 \cap K_2 \in \mathbb{S}$.

If for $F \in \mathbb{S}$ there exist exactly two $K_1, K_2 \in \mathcal{T}$ with $F = K_1 \cap K_2$, then F is called a *face*. We denote by \mathcal{F}_h the set of all faces which are m -dimensional linear manifolds, $0 \leq m \leq d-1$. For $d=3$ an element $E \in \mathbb{S}$ is called an edge of some $K \in \mathcal{T}$ if exactly two $F_1, F_2 \in \mathcal{F}_h$, $F_1, F_2 \subset K$ exist so that $E = F_1 \cap F_2$. We denote by \mathcal{E}_h the set of all edges. Finally, $\mathcal{N}_h = \{E_1 \cap E_2 : E_1, E_2 \in \mathcal{E}_h, E_1 \neq E_2\}$ is the set of *vertices*. A grid is conformal if \mathcal{E}_h and \mathcal{F}_h are conformal. Note that $\mathcal{F}_h = \mathcal{F}_{h,\Omega} \cup \mathcal{F}_{h,D} \cup \mathcal{F}_{h,N}$, where $\mathcal{F}_{h,\Omega}$, $\mathcal{F}_{h,D}$, and $\mathcal{F}_{h,N}$ denote the interior, Dirichlet, and Neumann faces respectively. In 2d, it holds that $\mathcal{E}_h = \mathcal{F}_h$. The set of mesh cells having a common face F is denoted by $\omega_F = \cup_{F \subset \partial K'} K'$ and ω_K denotes the patch of mesh cells that have a joint face with K .

Let $P(\mathcal{T})$ define a finite element space on our triangulation, then the functionals that define our finite element space are referred as *nodal functionals*. We denote by $N_F(\mathcal{T})$ the set of nodal functionals.

Remark 2. A finite element space can have different numbers of nodes and vertices, for, e.g., \mathbb{P}_2 Lagrange elements on simplices.

Remark 3. As we are concentrating on Lagrange elements each nodal functional can be determined by a point on the simplex, i.e., there is a one-to-one map between the functionals and the nodes on a simplex. By abuse of notations, we are denoting them by the same notation. If we need to make a distinction between the two, it will be explicitly stated.

Definition 4. (Conforming triangulation) A triangulation \mathcal{T} of Ω is called conforming if for $K_1, K_2 \in \mathcal{T}$ with $K_1 \neq K_2$ the intersection $K_1 \cap K_2$ is either empty, a vertex, an edge, or a 2- face of K_1 and K_2 .

Definition 5. (Refinement) ([Grä11, Definition 3.3]) Let \mathcal{T}_1 and \mathcal{T}_2 be triangulations of Ω . Then \mathcal{T}_2 is called a refinement of \mathcal{T}_1 if for all $K \in \mathcal{T}_1$ the set

$$\{K' \in \mathcal{T}_2 : K' \cap K \neq \emptyset\}$$

is a triangulation of K .

Definition 6. (Grid hierarchy) ([Grä11, Definition 3.4]) A family $\{\mathcal{T}_i\}_{i=0}^j$ is called a grid hierarchy on Ω if \mathcal{T}_0 is a conforming triangulation of Ω , and if each $\mathcal{T}_i, i = 1, \dots, j$, is a refinement of \mathcal{T}_{i-1} . If the grid \mathcal{T}_i is conforming we call it conforming grid refinement otherwise non-conforming grid refinement.

Remark 7. An interesting property of the grid hierarchy is the embedding of the set of vertices $\mathcal{N}_{hi} \subset \mathcal{N}_{h(i+1)}$.

Definition 8. (Hanging vertex) ([Grä11, Definition 3.6]) Let \mathcal{T} be a triangulation of Ω . Then a vertex $p \in \mathcal{N}_h(\mathcal{T})$ of \mathcal{T} is called a hanging vertex if there is an element $K \in \mathcal{T}$ with $p \in \partial K$ but p is not a vertex of K .

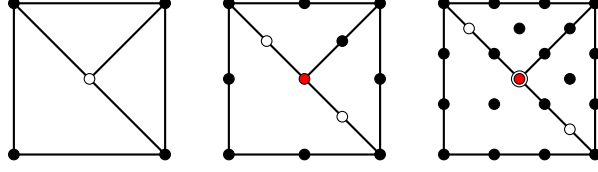


Figure 1: Hanging nodes and vertices for \mathbb{P}_1 , \mathbb{P}_2 , and \mathbb{P}_3 Lagrange elements. Hanging nodes in white and hanging vertices in red.

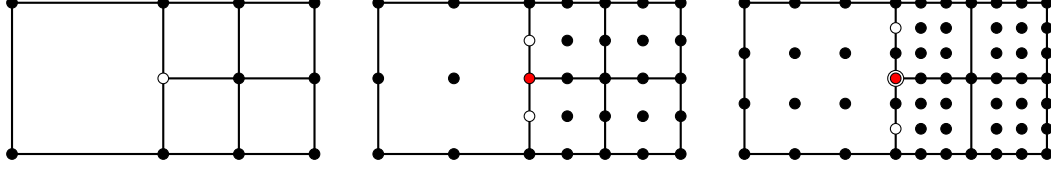


Figure 2: Hanging nodes and vertices for \mathbb{Q}_1 , \mathbb{Q}_2 , and \mathbb{Q}_3 Lagrange elements. Hanging nodes in white and hanging vertices in red.

Definition 9. (Hanging node) Let \mathcal{T} be a triangulation of Ω and $P(\mathcal{T})$ be a Lagrange finite element space defined on \mathcal{T} . Then a node $p \in N_F(\mathcal{T})$ of \mathcal{T} is called a hanging node if there is an element $K \in \mathcal{T}$, such that, $p \in K \cap K'$ and $p \in N_F(K)$ but $p \notin N_F(K')$ where K' is a neighbor of K . The set of all hanging nodes is denoted by $H(\mathcal{T})$.

Remark 10. Note that for \mathbb{P}_1 and \mathbb{Q}_1 elements the concepts of hanging vertex and hanging node match. But for \mathbb{P}_k or \mathbb{Q}_k elements, $k > 1$, they don't match see Fig. 1 and Fig. 2, where hanging nodes are shown with white color and hanging vertices by red.

3 Hanging nodes in theory of Lagrange elements

In this subsection we extend the results from [Gräll1] for hanging nodes from $\mathbb{P}_1/\mathbb{Q}_1$ elements to $\mathbb{P}_k/\mathbb{Q}_k$ elements.

Let \mathcal{T} be a conforming triangulation of Ω . For such a triangulation the k^{th} order Lagrangian finite element functions are continuous functions on $\overline{\Omega}$ such that the restrictions to all elements $K \in \mathcal{T}$ are polynomials with degree at most k . It is known that these function spaces are conforming subspaces with respect to $H^1(\Omega)$. However, the same definition also leads to conforming spaces if it is used on non-conforming triangulations.

Definition 11. (k^{th} order conforming space) Let \mathcal{T} be a triangulation of Ω . The k^{th} order conforming finite element space is defined as

$$S(\mathcal{T}) := \{v \in \mathcal{C}(\overline{\Omega}) : v|_K \in \mathbb{P}_k(K) \quad \forall K \in \mathcal{T}\} \subset H^1(\Omega).$$

For conforming triangulations a basis of $S(\mathcal{T})$ is given by the well-known nodal basis functions. To deal with conforming finite element spaces in non-conforming triangulation we first introduce the non-conforming nodal basis functions.

Definition 12. (Non-conforming nodal basis functions) Let \mathcal{T} be a triangulation of Ω . Then the non-conforming nodal basis function $\varphi_p^{\text{nc}} \in L^2(\Omega)$ associated with $p \in N_F(\mathcal{T})$ is defined as follows: For all $K \in \mathcal{T}$ there is a representative $\varphi_p^{\text{nc}}|_K = \mu_{p,K} \in \mathcal{C}(K)$ with $\mu_{p,K} = \delta_{pq}$ for all nodes q of K .

For a conforming triangulation \mathcal{T} this reduces to $\varphi_p^{\text{nc}} \in S(\mathcal{T})$ and

$$\varphi_p^{\text{nc}}(q) = \delta_{pq} \quad \forall p, q \in N_F(\mathcal{T}),$$

i.e., the set $\{\varphi_p^{\text{nc}}\}_{p \in N_F(\mathcal{T})}$ is the conforming nodal basis of $S(\mathcal{T})$. For a conforming triangulation, $S(\mathcal{T})$ is in general only a subspace of the non-conforming finite element space,

$$S^{\text{nc}}(\mathcal{T}) := \text{span}\{\varphi_p^{\text{nc}} : p \in N_F(\mathcal{T})\}.$$

However, for a non-conforming triangulation it is possible to construct a basis of $S(\mathcal{T})$ from the non-conforming nodal basis $S^{\text{nc}}(\mathcal{T})$ that resembles the usual nodal basis functions when \mathcal{T} is conforming.

Lemma 13. *Let \mathcal{T} be a non-conforming triangulation of Ω , i.e., \mathcal{T} has hanging nodes. Then, if $v \in S(\mathcal{T})$, then $\forall q \in H(\mathcal{T})$ there are coefficients a_{qp} with $p \in N_F(\mathcal{T}) \setminus H(\mathcal{T})$ such that,*

$$v(q) = \sum_{p \in N_F(\mathcal{T}) \setminus H(\mathcal{T})} a_{qp} v(p).$$

Proof. Let $q \in H(\mathcal{T})$. Suppose there does not exist any a_{qp} such that

$$v(q) = \sum_{p \in N_F(\mathcal{T}) \setminus H(\mathcal{T})} a_{qp} v(p).$$

As $q \in H(\mathcal{T})$, therefore there exists $K, K' \in \mathcal{T}$ such that $q \in K \cap K'$ and $q \in N_F(K)$ but $q \notin N_F(K')$.

Now,

$$v|_{K'}(x) = \sum_{p_0 \in N_F(K')} v(p_0) \varphi_{p_0}^{\text{nc}}(x),$$

as $q \in K'$

$$\Rightarrow v|_{K'}(q) = \sum_{p_0 \in N_F(K')} v(p_0) \varphi_{p_0}^{\text{nc}}(q).$$

Also, as $q \in K$ and $q \in N_F(K)$,

$$\Rightarrow v|_K(q) = v(q).$$

By continuity of v we have

$$v|_K(q) = v|_{K'}(q) \Rightarrow v(q) = \sum_{p_0 \in N_F(K')} v(p_0) \varphi_{p_0}^{\text{nc}}(q),$$

which is a contradiction and hence the result holds. \square

Remark 14. The proof of the Lemma 13 gives a concrete choice for the definition of a_{qp} . Namely $a_{qp} = \varphi_p^{\text{nc}}(q)$ where $p \in N_F(K')$ if $q \in N_F(K)$ and $q \in K \cap K'$.

Remark 15. If one would like the solution to be in $S(\mathcal{T})$, then one notes from Lemma 13 that the hanging nodes are not free but are dependent.

Theorem 16. ([Grä11, Theorem 3.1]) *Let $(\mathcal{T}_0, \dots, \mathcal{T}_j)$ be a grid hierarchy on Ω with \mathcal{T}_0 being conforming. Let us denote $\mathcal{T} = \mathcal{T}_j$, i.e., the final refinement level. Then a basis of $S(\mathcal{T})$ is given by*

$$B(\mathcal{T}) := \left\{ \varphi_p = \varphi_p^{\text{nc}} + \sum_{q \in H(\mathcal{T})} a_{qp} \varphi_q^{\text{nc}} : p \in N_F(\mathcal{T}) \setminus H(\mathcal{T}) \right\}.$$

Proof. The proof from [Grä11] can be extended to higher order elements without any changes. \square

4 Hanging nodes in theory of AFC schemes

In this subsection we discuss the implementation of hanging nodes for the AFC schemes, the failure of satisfaction of DMP with hanging nodes for the Kuzmin limiter and the modification for the BJK limiter.

4.1 Implementation of hanging nodes

The implementation of hanging nodes is a little bit similar to the implementation of Dirichlet nodes, i.e., it works on an algebraic level. Let us denote our finite element matrix on a non-conforming grid by A^{nc} and the corresponding right-hand side by b^{nc} . Hence, our finite problem is to find $u \in S^{\text{nc}}(\mathcal{T})$ such that

$$A^{\text{nc}} u = b^{\text{nc}},$$

where $S^{\text{nc}}(\mathcal{T})$ is a finite element space defined on \mathcal{T} . Here A^{nc} and b^{nc} are derived using discontinuous elements from $S^{\text{nc}}(\mathcal{T})$ and hence our solution is discontinuous as well. To restore the continuity of the finite element solution, we look at the variational form of the problem. Let $a_h^{\text{nc}} : S^{\text{nc}}(\mathcal{T}) \times S^{\text{nc}}(\mathcal{T}) \rightarrow \mathbb{R}$ be the corresponding bilinear form and f_h be the right-hand side, then our problem is

$$a_h^{\text{nc}}(u, v) = \langle f_h, v \rangle \quad \forall v \in S^{\text{nc}}(\mathcal{T}).$$

First we modify our test space and replace $S^{\text{nc}}(\mathcal{T})$ by $S(\mathcal{T})$. Then

$$a_h^{\text{nc}}(u, v) = \langle f_h, v \rangle \quad \forall v \in S(\mathcal{T}).$$

The algebraic form of the above problem can be written as

$$\bar{A}u = \bar{b},$$

where the right-hand side is assembled using continuous elements. To enforce continuity on the solution we modify the stiffness matrix for the hanging nodes in the same way as that for the Dirichlet nodes, i.e., we modify the rows corresponding to hanging nodes such that the solution at hanging node is continuous with respect to the coupling nodes and set the corresponding right-hand side to zero. Till this point the implementation of hanging nodes is general and can be applied to any higher order elements.

For the AFC scheme, in the first step, a system is assembled that corresponds to a Galerkin finite element discretization of the given equations but with Neumann boundary conditions on the whole boundary. For implementation with hanging nodes, \bar{A} is used to define D and after the computation of limiters, \bar{A} is modified to A with correct entries for hanging rows, where the rows of non-hanging nodes get entries from the rows of the hanging nodes.

Example 17. Implementation for \mathbb{P}_1 elements We will take a patch as defined in Fig. 3 and see how does the stiffness matrix and the right-hand side modify. Initially the system is

$$A^{\text{nc}}u = b^{\text{nc}},$$

where

$$A^{\text{nc}} = \begin{bmatrix} a_{00} & a_{01} & a_{02} & a_{03} & a_{04} \\ a_{10} & a_{11} & a_{12} & a_{13} & a_{14} \\ a_{20} & a_{21} & a_{22} & a_{23} & a_{24} \\ a_{30} & a_{31} & a_{32} & a_{33} & a_{34} \\ a_{40} & a_{41} & a_{42} & a_{43} & a_{44} \end{bmatrix}, \quad b^{\text{nc}} = \begin{bmatrix} b_0 \\ b_1 \\ b_2 \\ b_3 \\ b_4 \end{bmatrix}.$$

First, we modify A^{nc} and b^{nc} to \bar{A} and \bar{b} by performing row transformations $R_1 \rightarrow R_1 + 0.5R_0$ and $R_3 \rightarrow R_3 + 0.5R_0$, then

$$\bar{A} = \begin{bmatrix} a_{00} & a_{01} & a_{02} & a_{03} & a_{04} \\ a_{10} + \frac{a_{00}}{2} & a_{11} + \frac{a_{01}}{2} & a_{12} + \frac{a_{02}}{2} & a_{13} + \frac{a_{03}}{2} & a_{14} + \frac{a_{04}}{2} \\ a_{20} & a_{21} & a_{22} & a_{23} & a_{24} \\ a_{30} + \frac{a_{00}}{2} & a_{31} + \frac{a_{01}}{2} & a_{32} + \frac{a_{02}}{2} & a_{33} + \frac{a_{03}}{2} & a_{34} + \frac{a_{04}}{2} \\ a_{40} & a_{41} & a_{42} & a_{43} & a_{44} \end{bmatrix}, \quad \bar{b} = \begin{bmatrix} b_0 \\ b_1 + \frac{b_0}{2} \\ b_2 \\ b_3 + \frac{b_0}{2} \\ b_4 \end{bmatrix}.$$

At this step the computation of the limiters in AFC is performed using \bar{A} and \bar{b} . Once, the computation is done we modify the hanging row to $(1, -0.5, 0, -0.5, 0)$,

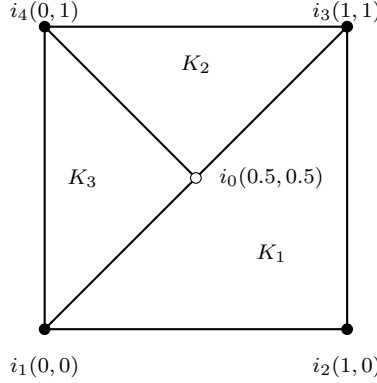


Figure 3: Example of a patch failing non-positivity condition for the Kuzmin limiter.

where -0.5 appears on the coupling nodes and correspondingly set the right-hand side to 0. Finally, our system of equations is

$$Au = b$$

where

$$A = \begin{bmatrix} 1 & -\frac{1}{2} & 0 & -\frac{1}{2} & 0 \\ \check{a}_{10} + \frac{\check{a}_{00}}{2} & \check{a}_{11} + \frac{\check{a}_{01}}{2} & \check{a}_{12} + \frac{\check{a}_{02}}{2} & \check{a}_{13} + \frac{\check{a}_{03}}{2} & \check{a}_{14} + \frac{\check{a}_{04}}{2} \\ \check{a}_{20} & \check{a}_{21} & \check{a}_{22} & \check{a}_{23} & \check{a}_{24} \\ \check{a}_{30} + \frac{\check{a}_{00}}{2} & \check{a}_{31} + \frac{\check{a}_{01}}{2} & \check{a}_{32} + \frac{\check{a}_{02}}{2} & \check{a}_{33} + \frac{\check{a}_{03}}{2} & \check{a}_{34} + \frac{\check{a}_{04}}{2} \\ \check{a}_{40} & \check{a}_{41} & \check{a}_{42} & \check{a}_{43} & \check{a}_{44} \end{bmatrix}, \quad b = \begin{bmatrix} 0 \\ \check{b}_1 + \frac{\check{b}_0}{2} \\ \check{b}_2 \\ \check{b}_3 + \frac{\check{b}_0}{2} \\ \check{b}_4 \end{bmatrix}.$$

Remark 18. Depending on the iterative scheme for solving the nonlinear problem, the matrix or the right-hand side change because of the contribution from the limiter (see [JJ19]). Hence, instead of $\{a_{ij}\}$ or $\{b_i\}$, one gets $\{\check{a}_{ij}\}$ or $\{\check{b}_i\}$.

4.2 Kuzmin Limiter

In [BJK16], the proof of discrete maximum principle (DMP) for the Kuzmin limiter relies on the assumption of the type $a_{kl} + a_{lk} \leq 0$ where a_{kl} belongs to the stiffness matrix \bar{A} defined previously. For *convection-diffusion-reaction* equations on conforming grids this condition is satisfied if and only if $(\nabla\varphi_l, \nabla\varphi_k) \leq 0$, which leads to the Delaunay condition (see [BJK16, Remark 14]). For non-conforming grids we don't have such a generalization. One needs to check this condition individually for all nodes. The next example presents a patch in 2d where this condition fails.

Example 19. Let's take a simple 2d example of *convection-diffusion-reaction* equations with some diffusion, ε , convection, $\mathbf{b} = (b_1, b_2)$, and reaction, $c = 0$ on

the patch as shown in Fig. 3. Then our non-conforming nodal basis functions $\{\varphi_{i_j}^{\text{nc}}\}_{j=0}^4$ are given by

$$\begin{aligned}\varphi_{i_0}^{\text{nc}} &= \begin{cases} 0 & \text{in } K_1, \\ 2-2y & \text{in } K_2, \\ 2x & \text{in } K_3, \end{cases} \quad \varphi_{i_1}^{\text{nc}} = \begin{cases} 1-x & \text{in } K_1, \\ 0 & \text{in } K_2, \\ 1-x-y & \text{in } K_3, \end{cases} \\ \varphi_{i_2}^{\text{nc}} &= \begin{cases} x-y & \text{in } K_1, \\ 0 & \text{in } K_2, \\ 0 & \text{in } K_3, \end{cases} \quad \varphi_{i_3}^{\text{nc}} = \begin{cases} y & \text{in } K_1, \\ x+y-1 & \text{in } K_2, \\ 0 & \text{in } K_3, \end{cases} \\ \varphi_{i_4}^{\text{nc}} &= \begin{cases} 0 & \text{in } K_1, \\ -x+y & \text{in } K_2, \\ -x+y & \text{in } K_3. \end{cases}\end{aligned}$$

After the coupling the conforming nodal basis functions, φ_{i_1} and φ_{i_3} look like

$$\varphi_{i_1} = \varphi_{i_1}^{\text{nc}} + \frac{1}{2}\varphi_{i_0}^{\text{nc}} = \begin{cases} 1-x & \text{in } K_1, \\ 1-y & \text{in } K_2, \\ 1-y & \text{in } K_3, \end{cases} \quad \varphi_{i_3} = \varphi_{i_3}^{\text{nc}} + \frac{1}{2}\varphi_{i_0}^{\text{nc}} = \begin{cases} y & \text{in } K_1, \\ x & \text{in } K_2, \\ x & \text{in } K_3. \end{cases}$$

For rest of the nodes there are not any contributions from the hanging nodes and hence $\varphi_{i_j} = \varphi_{i_j}^{\text{nc}}$ for $j = 0, 2, 4$. We need to check the sign of $a_{i_1 i_3} + a_{i_3 i_1}$. From the bilinear form we have

$$\begin{aligned}a_{i_1 i_3} + a_{i_3 i_1} &= a_{31} + \frac{1}{2}a_{01} + a_{13} + \frac{1}{2}a_{03} \\ &= \varepsilon (\nabla \varphi_{i_3}^{\text{nc}}, \nabla \varphi_{i_1}) + (\mathbf{b} \cdot \nabla \varphi_{i_3}^{\text{nc}}, \varphi_{i_1}) \\ &\quad + \varepsilon (\nabla \varphi_{i_1}^{\text{nc}}, \nabla \varphi_{i_3}) + (\mathbf{b} \cdot \nabla \varphi_{i_1}^{\text{nc}}, \varphi_{i_3}).\end{aligned}$$

The gradients of the basis functions required in the above computation are given by

$$\begin{aligned}\nabla \varphi_{i_1}^{\text{nc}} &= \begin{cases} (-1, 0) & \text{in } K_1, \\ (0, 0) & \text{in } K_2, \\ (-1, -1) & \text{in } K_3, \end{cases} \quad \nabla \varphi_{i_3}^{\text{nc}} = \begin{cases} (0, 1) & \text{in } K_1, \\ (1, 1) & \text{in } K_2, \\ (0, 0) & \text{in } K_3, \end{cases} \\ \nabla \varphi_{i_1} &= \begin{cases} (-1, 0) & \text{in } K_1, \\ (0, -1) & \text{in } K_2, \\ (0, -1) & \text{in } K_3, \end{cases} \quad \nabla \varphi_{i_3} = \begin{cases} (0, 1) & \text{in } K_1, \\ (1, 0) & \text{in } K_2, \\ (1, 0) & \text{in } K_3, \end{cases}\end{aligned}$$

Finally consider the sum $a_{i_1 i_3} + a_{i_3 i_1}$,

$$\begin{aligned}a_{i_1 i_3} + a_{i_3 i_1} &= -\varepsilon (|K_2| + |K_3|) + b_2 \int_{K_1} (1-x)ds + (b_1 + b_2) \int_{K_2} (1-y)ds \\ &\quad - b_1 \int_{K_1} yds - (b_1 + b_2) \int_{K_3} xds \\ &= \frac{-3\varepsilon}{4} + \frac{(b_2 - b_1)}{3}.\end{aligned}$$

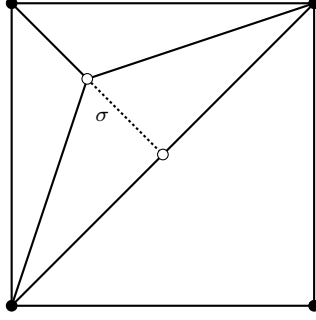


Figure 4: Hanging node being a limit of a non-Delaunay grid as $\sigma \rightarrow 0$.

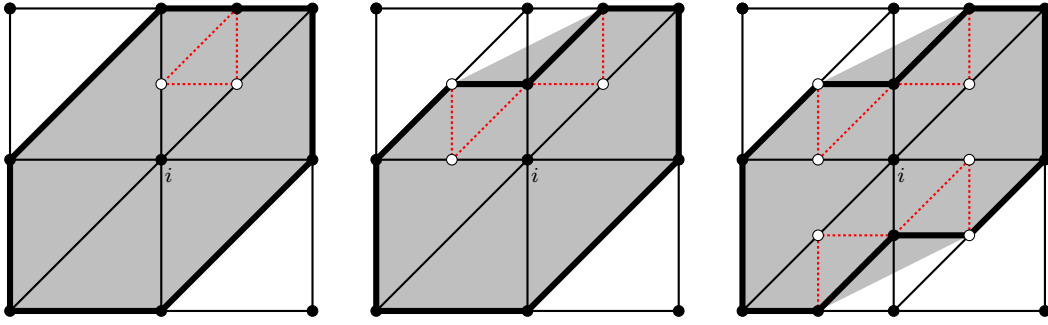


Figure 5: Examples of Δ_i for the node x_i with bold lines and Δ_i^{conv} with the shaded area.

For $\varepsilon \leq 0.1$ and $\mathbf{b} = (0, 1)$ we have $a_{i_1 i_3} + a_{i_3 i_1} > 0$.

Remark 20. One can consider the situation of a hanging node in Fig. 3 as the limit of a non-Delaunay grid and in this respect, this property of the Kuzmin limiter is not surprising (see Fig. 4).

4.3 BJK Limiter

We have another definition for the limiter, where the proof of DMP holds for all conforming simplicial grids. This is the BJK limiter defined in [BJK17]. Here the condition of the DMP relies on the properties of the stiffness matrix instead on the triangulation. Let us assume that the condition

$$\sum_{j=1}^N a_{ij} \geq 0, \quad i = 1, \dots, M$$

is satisfied. Let Δ_i denote $\text{supp}(\varphi_i)$. Examples of Δ_i for x_i are shown in Fig. 5 with bold lines and their convex hull, Δ_i^{conv} , by the shaded area. In [BJK17], for conforming grids, Δ_i denoted the patch having the node x_i .

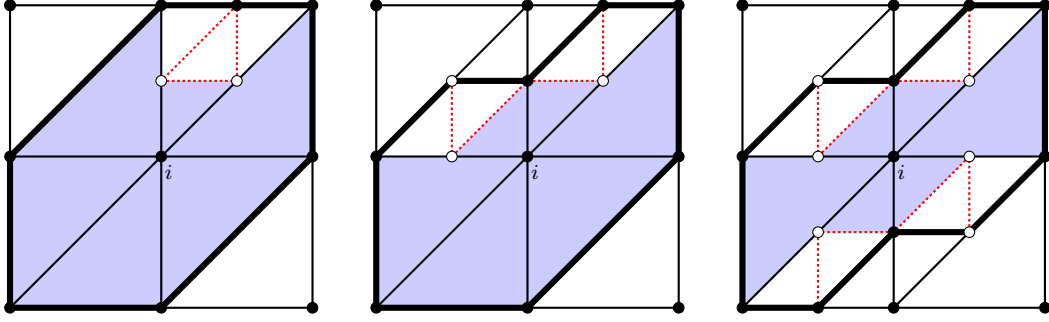


Figure 6: Examples of $\Delta_i^{T,\text{conv}}$ for the node x_i .

Remark 21. One of the main assumptions for AFC schemes is the positivity of the row sum, i.e., $\sum_{j=1}^N a_{ij} \geq 0$ (see [BJK17, Eq. (2.6)], [BJK16, Eq. (8)]). With the use of hanging nodes, this condition is still satisfied, as the positivity of row sum is not affected by adding a positive multiple of a row to another row.

Remark 22. For the computation of the limiters a certain constant γ_i is required to show linearity preservation. From [BJK17, Theorem 6.1] the definition of γ_i is given by

$$\gamma_i = \frac{\max_{x_j \in \partial\Delta_i} |x_i - x_j|}{\text{dist}(x_i, \partial\Delta_i^{\text{conv}})}, \quad i = 1, \dots, M.$$

The computation of the numerator is easy as compared to the computation of the denominator. For simplices, ideas on computation of Δ_i are given by [BJK17, Remark 6.2]. With hanging nodes the shape of Δ_i is not a polygon made of a union of triangles sharing the node x_i but a generalized polygon (in 2d). This computation is more involved. In our simulations, for the denominator we consider Δ_i as all those triangles which share the vertex x_i . Let us denote it by $\Delta_i^{T,\text{conv}}$, see Fig. 6. This definition leads to

$$\text{dist}(x_i, \partial\Delta_i^{T,\text{conv}}) \leq \text{dist}(x_i, \partial\Delta_i^{\text{conv}}),$$

hence, the value used in simulations might be larger than γ_i . From the theory of conforming grids, it is known that the DMP is satisfied if this parameter is larger than γ_i .

Remark 23. The example patches that we have shown are for structured grids that will be used in our simulations. As the BJK limiter can be applied to unstructured grids, we may have presence of triangles of varying sizes and hence requiring generalizations. We would not consider that case in this work, as we need to assume certain shape regularity on the initial grid for the underlying a posteriori error estimates. The analysis for AFC schemes with anisotropic grids remain an open problem [BJKR18].

4.4 Limiter Definition

One last thing we want to note is what should be α_{ij} for a hanging node x_i . First, the idea for Dirichlet nodes was used, i.e., $\alpha_{ij} = 1$ for each hanging node x_i . This choice leads to some overshoots. The possible reason being the presence of hanging nodes in the layer and the absence of the artificial diffusion as $\alpha_{ij} = 1$ leads to standard Galerkin method. Hence, we choose $\alpha_{ij} = 0$ for hanging node x_i . This is an overly diffusive approach at least locally. This issue will be studied in the numerical simulations. One should note that none of the applied estimators was derived for grids with hanging nodes.

5 Numerical studies

The numerical studies presented in this section validates the results presented in the previous section. We will use a posteriori error estimators defined in [Jha20]. In [Jha20], two different techniques for the upper bound were proposed in the energy norm of the error, one used a residual-based approach which we refer to as *AFC-energy* technique and the second approach used the SUPG solution and the SUPG estimators from [JN13], which will be referred as *AFC-SUPG-energy* technique. For brevity we are omitting the detailed description of the a posteriori error estimator.

For simulations the matrices were assembled exactly and the linear systems were solved using the direct solver UMFPACK [Dav04]. The method fixed point rhs was used for solving the nonlinear problems with the damping parameters as described in [JJ19]. All the simulations were performed with the in-house code ParMooN [WBA⁺16].

Example with interior and boundary layer This example was presented in [HMM86]. It is given in $\Omega = (0, 1)^2$ with $\mathbf{b} = (\cos(-\pi/3), \sin(-\pi/3))$, $c = f = 0$ and the Dirichlet boundary condition

$$u_b = \begin{cases} 1 & (y = 1 \wedge x > 0) \text{ or } (x = 0 \wedge y > 0.7), \\ 0 & \text{else.} \end{cases}$$

Here, the convection-dominated case $\varepsilon = 10^{-4}$ is considered. We know that, the solution exhibits an internal layer in the direction of the convection starting from the jump of the boundary condition at the left boundary and two exponential layers at the right and the lower boundary (see Fig. 7). An analytic solution to this problem is not available but we know that $u \in [0, 1]$. Hence, this example will help us in showing the violation or satisfaction of the DMP with grids containing hanging nodes. This example will also help in checking the quality of the adaptively refined grids.

To show the violation of DMP, we define a function

$$\text{Var}(u_h) := u_h^{\max} - u_h^{\min}. \quad (1)$$

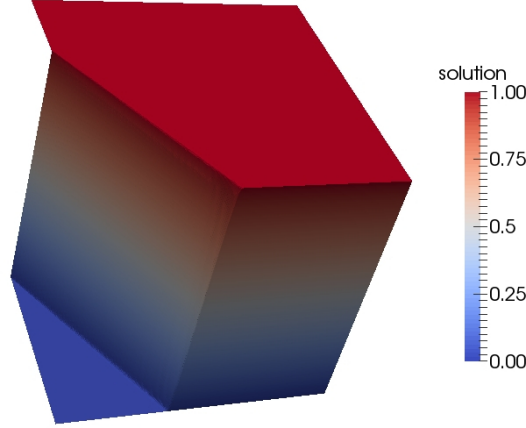


Figure 7: 2d Interior and boundary layer example. Solution (computed with the BJK limiter, level 9).

Due to boundary conditions, $u_h^{\max} \geq 1$ and $u_h^{\min} \leq 0$, hence $\text{Var}(u_h) \geq 1$. As, the solution $u \in [0, 1]$, one would expect $\text{Var}(u_h) \approx 1$ for all grids.

An initial mesh was defined with two triangles by joining the points $(0, 0)$ and $(1, 1)$. The simulations were started with a level 2 grid (i.e., $\#\text{dof} = 25$), initially uniform refinement was performed till level 4 (i.e., $\#\text{dof} = 289$). After that adaptive refinement was performed. AFC schemes are applicable to first order elements, hence \mathbb{P}_1 finite elements were used.

First, we study the behavior of $\text{Var}(u_h)$ for the *AFC-energy* technique. For the Kuzmin limiter we see a violation of DMP on grids with hanging nodes but satisfaction on grids with conforming closure (see Fig. 8 (left)). The failure of DMP is not surprising as this behavior was predicted in Sec. 4. Whereas, for the BJK limiter, we observe the satisfaction of DMP on both kinds of grids (see Fig. 9 (left)). Next, we study the behavior of $\text{Var}(u_h)$ for the *AFC-SUPG-energy* technique. The results are similar to the results for *AFC-energy* technique for grids with hanging nodes, that is, failure of the DMP with Kuzmin limiter (see Fig. 8 (right)) and satisfaction of the DMP with the BJK limiter (see Fig. 9 (right)). For grids with conforming closures the results are similar to the *AFC-energy* technique.

Now, we consider the adaptive grid refinements. The 14th adaptively refined grids with conforming closure are shown in Fig. 10 for both the techniques. Here we see that we have the presence of non-Delaunay triangulations and still the satisfaction of DMP for the Kuzmin limiter. Comparing the refinement for both the limiters, we observe that more mesh cells are refined for the BJK limiter as compared to the Kuzmin limiter (see Fig. 10 for $\#\text{dof}$). For the *AFC-SUPG-energy* technique (see Fig. 10 (bottom left) for the Kuzmin limiter and (bottom right) for the BJK limiter) we observe that the mesh cells near the internal layer are not refined that much as compared to the *AFC-energy* technique. Also, we

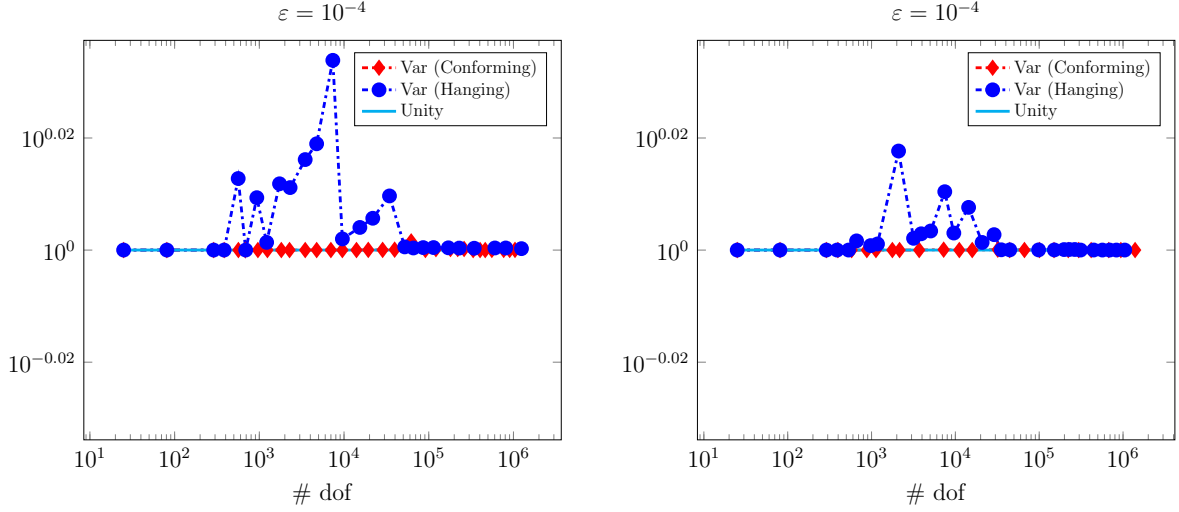


Figure 8: Variation for the Kuzmin limiter as defined in (1). *AFC-energy* technique (left), *AFC-SUPG-energy* technique (right)

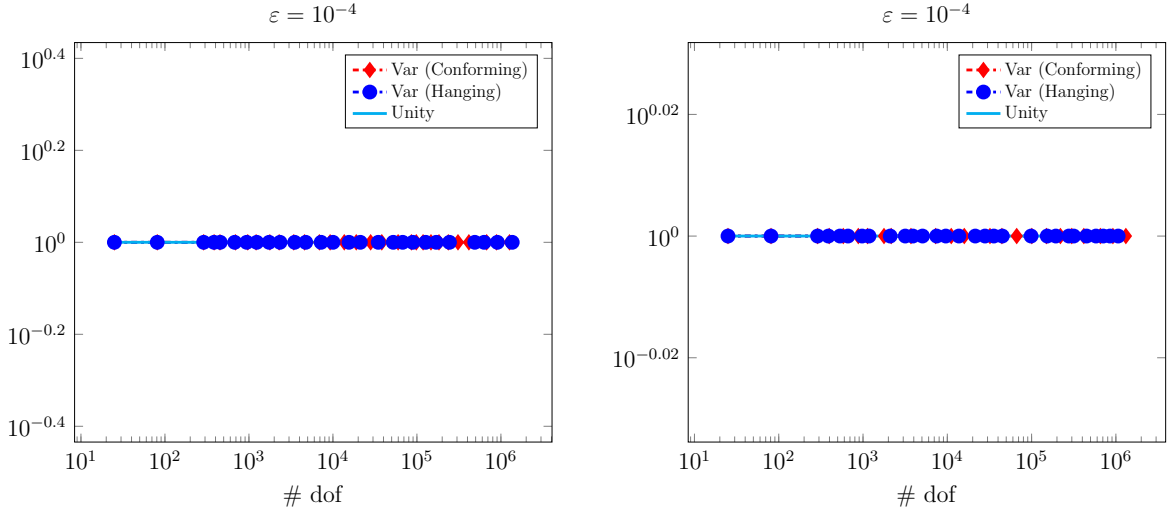


Figure 9: Variation for the BJK limiter as defined in (1). *AFC-energy* technique (left), *AFC-SUPG-energy* technique (right)

see that the limiters do not play an important role in the adaptive refinement.

The 14th adaptively refine grids with hanging nodes are shown in Fig. 11. For the *AFC-energy* technique comparing the refinement for both the limiters, we observe that both the meshes are comparable (see Fig. 11 for all and hanging #dof). Here, all #dof refer to boundary+hanging+interior degrees of freedom, whereas hanging #dof refers to the hanging nodes. With the *AFC-SUPG-energy* technique we observe that the mesh cells near the internal layer are not refined that much as compared to the *AFC-energy* technique. Similar to conformally

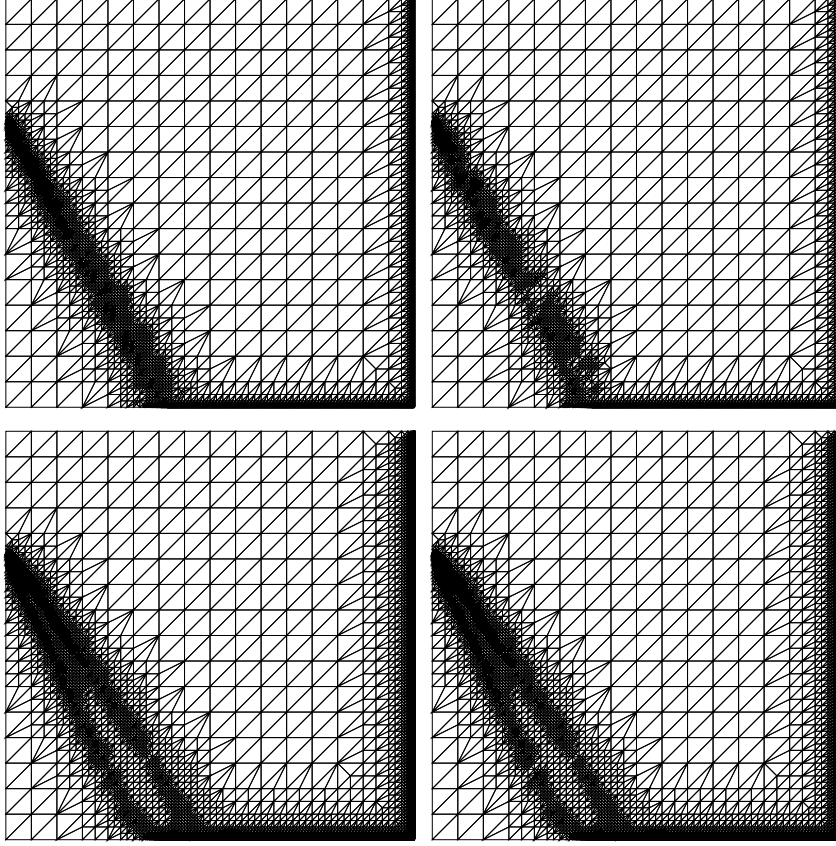


Figure 10: 14th adaptively refined grid with conforming closure. Kuzmin limiter+*AFC-energy* technique (14th grid: #dof = 19325 (top left); BJK limiter+*AFC-energy* technique (14th grid: #dof = 28120 (top right) and Kuzmin limiter+*AFC-SUPG-energy* technique (14th grid: #dof = 100620 (bottom left); BJK limiter+*AFC-SUPG-energy* technique (14th grid: #dof = 100538 (bottom right)).

closed grids, the limiters do not play an important role in the refinement of the grid.

To check the thickness of the interior layer we follow the idea described in [JK07, Eq. (48)]. We define

$$smear_{\text{int}} = x_2 - x_1,$$

where x_1 is the x -coordinate of the first point on the cut line $(x, 0.25)$ with $u_h(x_1, 0.25) \geq 0.1$ and x_2 is the x -coordinate of the first point with $u_h(x_2, 0.25) \geq 0.9$. We note that in Fig. 12, the layers are most properly resolved on conformally closed grids for both the techniques. Overall, for adaptive grid refinement, the *AFC-energy* technique does a much better job since all layers are refined properly, not only the strongest layer. We note that the layers are better approximated

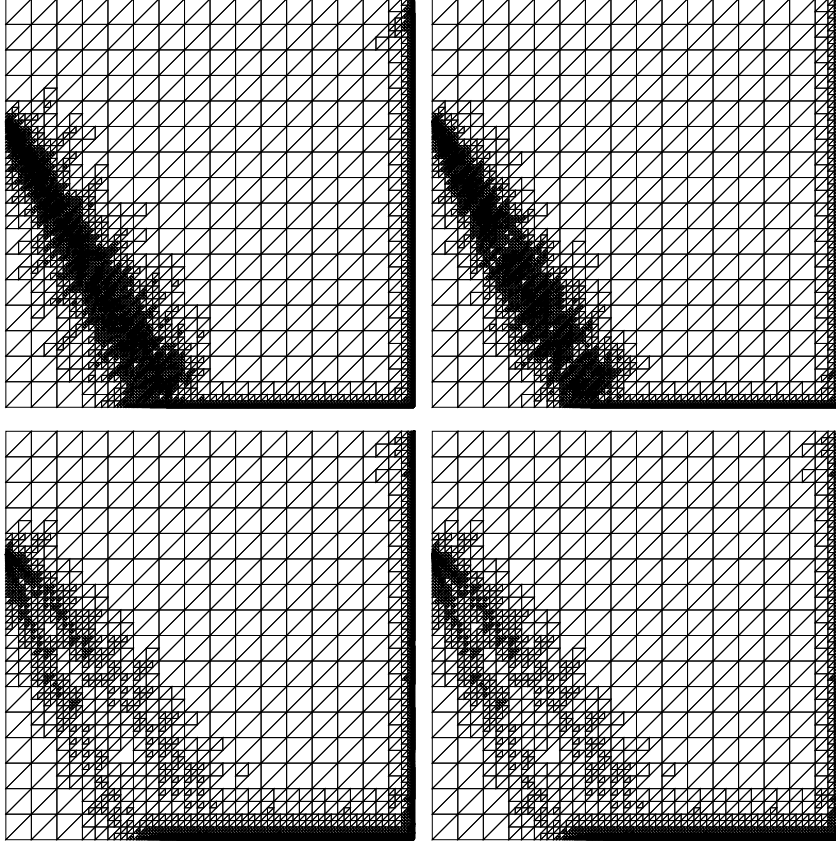


Figure 11: 14th adaptively refined grid with hanging nodes.

Kuzmin limiter+*AFC-energy* technique (14th grid: all #dof = 34418 , hanging #dof = 10493 (top left); BJK limiter+*AFC-energy* technique (14th grid: all #dof = 34633, hanging #dof = 11029 (top right) and Kuzmin limiter+*AFC-SUPG-energy* technique (14th grid: all #dof = 28961 , hanging #dof = 7027 (top left); BJK limiter+*AFC-SUPG-energy* technique (14th grid: all #dof = 28027, hanging #dof = 6657 (top right).

on conformally closed grids as compared to the grids with hanging nodes for the *AFC-SUPG-energy* technique.

6 Summary

This is the first work in the direction of hanging nodes in context of non-linear stabilization for convection-diffusion equations. This chapter dealt with two aspects of hanging nodes. First, results have been extended from lower-order Lagrange elements to higher-order elements. Second, we studied the behavior of AFC schemes on grids with hanging nodes.

The following conclusions can be made from the numerical simulations

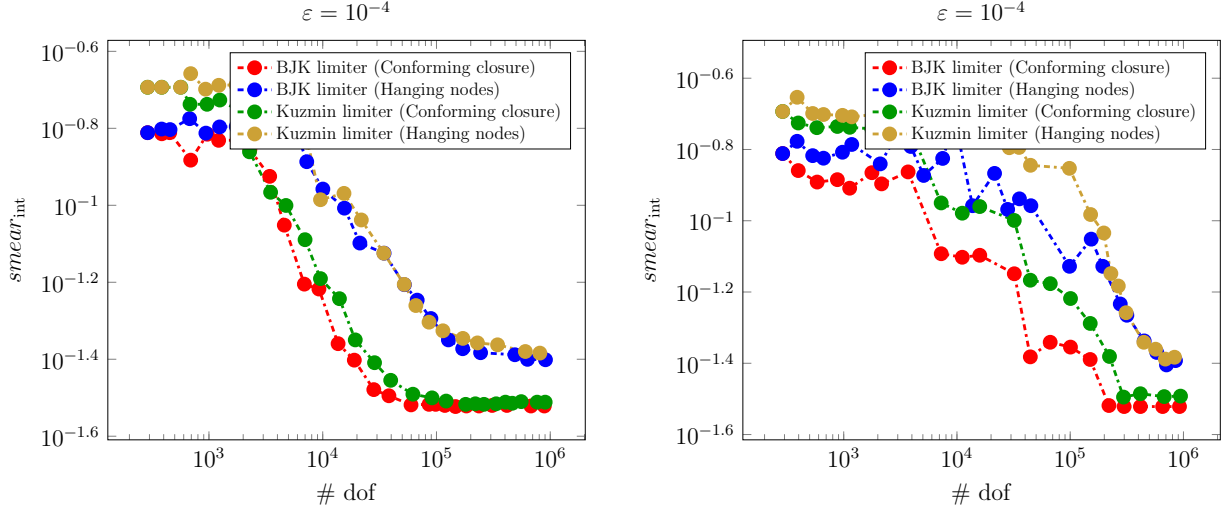


Figure 12: Thickness of internal layer. *AFC-energy* technique (left), *AFC-SUPG-energy* technique (right)

1. The Kuzmin limiter fails to satisfy the DMP for both the estimators on grids with hanging nodes. A concrete example was provided which justified this behavior.
2. The Kuzmin limiter satisfies DMP for both the estimators on grids with conforming closure, even though there is the presence of non-Delaunay triangulation.
3. The BJK limiter satisfies the DMP for both the estimators on all kinds of grids, i.e., conformally closed grids as well as grids with hanging nodes.
4. The layers were better resolved on conformally closed grids as compared to grids with hanging nodes, irrespective of the choice of limiters.

In summary, the numerical results on grids with hanging nodes are not satisfactory and one should find alternative ways for grid refinements in three dimension and should not continue to work in this direction.

7 Acknowledgements

The work of the author has been supported by Berlin Mathematical School (BMS). The author would like to thank Prof. Dr. Volker John for many fruitful discussions and suggestions.

References

- [AR10] Mark Ainsworth and Richard Rankin. Fully computable error bounds for discontinuous Galerkin finite element approximations on meshes with an arbitrary number of levels of hanging nodes. *SIAM J. Numer. Anal.*, 47(6):4112–4141, 2010.
- [BJK16] Gabriel R. Barrenechea, Volker John, and Petr Knobloch. Analysis of algebraic flux correction schemes. *SIAM J. Numer. Anal.*, 54(4):2427–2451, 2016.
- [BJK17] Gabriel R. Barrenechea, Volker John, and Petr Knobloch. An algebraic flux correction scheme satisfying the discrete maximum principle and linearity preservation on general meshes. *Math. Models Methods Appl. Sci.*, 27(3):525–548, 2017.
- [BJKR18] Gabriel R. Barrenechea, Volker John, Petr Knobloch, and Richard Rankin. A unified analysis of algebraic flux correction schemes for convection-diffusion equations. *SeMA J.*, 75(4):655–685, 2018.
- [BSW83] Randolph E. Bank, Andrew H. Sherman, and Alan Weiser. Refinement algorithms and data structures for regular local mesh refinement. In *Scientific computing (Montreal, Que., 1982)*, IMACS Trans. Sci. Comput., I, pages 3–17. IMACS, New Brunswick, NJ, 1983.
- [CH09] C. Carstensen and J. Hu. Hanging nodes in the unifying theory of a posteriori finite element error control. *J. Comput. Math.*, 27(2-3):215–236, 2009.
- [Dav04] Timothy A. Davis. Algorithm 832: UMFPACK V4.3—an unsymmetric-pattern multifrontal method. *ACM Trans. Math. Software*, 30(2):196–199, 2004.
- [Grä11] Carsten Gräser. *Convex minimization and phase field models*. PhD thesis, Freie Universität, Berlin, 2011.
- [HMM86] Thomas J. R. Hughes, Michel Mallet, and Akira Mizukami. A new finite element formulation for computational fluid dynamics. II. Beyond SUPG. *Comput. Methods Appl. Mech. Engrg.*, 54(3):341–355, 1986.
- [Jha20] Abhinav Jha. A Residual Based A Posteriori Error Estimators for AFC Schemes for Convection-Diffusion Equations. *arXiv e-prints*, page arXiv:2005.02938, May 2020.

- [JJ19] Abhinav Jha and Volker John. A study of solvers for nonlinear AFC discretizations of convection-diffusion equations. *Comput. Math. Appl.*, 78(9):3117–3138, 2019.
- [JK07] Volker John and Petr Knobloch. On spurious oscillations at layers diminishing (SOLD) methods for convection-diffusion equations. I. A review. *Comput. Methods Appl. Mech. Engrg.*, 196(17-20):2197–2215, 2007.
- [JN13] Volker John and Julia Novo. A robust SUPG norm a posteriori error estimator for stationary convection-diffusion equations. *Comput. Methods Appl. Mech. Engrg.*, 255:289–305, 2013.
- [KR89] Ralf Kornhuber and Rainer Roitzsch. On adaptive grid refinement in the presence of internal or boundary layers. Technical Report SC-89-05, ZIB, Takustr. 7, 14195 Berlin, 1989.
- [Riv84] María-Cecilia Rivara. Mesh refinement processes based on the generalized bisection of simplices. *SIAM J. Numer. Anal.*, 21(3):604–613, 1984.
- [WBA⁺16] U. Wilbrandt, C. Bartsch, N. Ahmed, N. Alia, F. Anker, L. Blank, A. Caiazzo, S. Ganesan, S. Giere, G. Matthies, R. Meesala, A. Shamim, J. Venkatesan, and V. John. Parmoon a modernized program package based on mapped finite elements. *Computers and Mathematics with Applications*, 74:74–88, 2016.
- [XZ99] Jinchao Xu and Ludmil Tomov Zikatanov. A monotone finite element scheme for convection-diffusion equations. *Mathematics of Computation*, 68(228):1429–1446, 10 1999.